A STUDY OF THE MATRIX DISPLACEMENT METHOD AS APPLIED TO SHELLS OF REVOLUTION

Stanley Klein*

Aerospace Corporation
San Bernardino Operations
San Bernardino, California

The paper describes the particular application of the matrix displacement finite element approach to the linear elastic analysis of shells of revolution under axisymmetric and asymmetric loads. The shell is idealized as a series of conical frusta, joined at nodal circles. The external forces are applied at the nodal circles. Problems encountered in the development of the method are discussed in detail and solutions to the various difficulties are outlined. Computer codes based on this technique are used to obtain a variety of solutions for simple and complex shell structures. These solutions illustrate the accuracy of the method in addition to indicating sources of error pertaining to the modeling technique employed for different shells. Improvements of the computer codes, methods of increasing the number of finite elements allowed, machine computation time required, and extensions of the analysis are all topics discussed in depth.

SYMBOLS

$A_{\alpha,\beta}$	Integrals defined in Equation 15
A	Surface area
B	Matrix of coefficients relating $\tilde{q}^i$ and α^i for an element
E	Young's modulus
E	Matrix of coefficients in the stress-strain relations, (Equation 7)
E*	Matrix of coefficients introduced in Equation 8
F	Column vector of applied generalized forces and reactions
K	Stiffness matrix for a structure
L	Matrix of coefficients introduced in Equation 9
M_s, M_θ, $M_{s\theta}$	Stress couples of shell
N_s, N_θ, $N_{s\theta}$	Stress resultants of shell
Q_s, Q_θ	Meridional shear stress resultants of shell
Q, $\bar{Q}$	Generalized forces; Fourier cosine and sine coefficients

*Member of the Technical Staff

SYMBOLS (Cont'd)

$T(\theta)$	Applied load per unit length at a node
U	Strain energy of element for assumed displacement field
W	Mechanical work
$\mathbf{w}^i$	Matrix of coefficients relating $\boldsymbol{\epsilon}^i$ and $\boldsymbol{\alpha}^i$ for an element
$f(s)$	Function of s
h	Shell thickness
i	Superscript denoting harmonic number
j	Subscript denoting generalized coordinate number
$\mathbf{k}$, $\tilde{\mathbf{k}}$	Stiffness matrix for element, referred to system coordinates and shell coordinates, respectively
ℓ	Meridional length of a conical element
p	Subscript denoting node number
q_j , $\bar{q}_j$	Generalized displacements j; Fourier cosine and sine coefficients
$\mathbf{q}^i$, $\tilde{\mathbf{q}}^i$	Column vectors of generalized displacements for harmonic number i, referred to system and shell coordinates, respectively
r	Radial coordinate
s	Meridional coordinate
u, v, w	Axial, circumferential, radial displacement
$\tilde{u}, \tilde{v}, \tilde{w}$	Meridional, circumferential, normal displacement
z	Axial coordinate
α_j^i	Coefficients introduced in Equation 5
β	Rotation of meridian
$\boldsymbol{\epsilon}$	Column vector of strain components at a point in shell surface
ϵ_s , ϵ_θ , $\epsilon_{s\theta}$	Strains of the shell surface
θ	Circumferential angle, coordinate
κ_s , κ_θ , $\kappa_{s\theta}$	Curvature changes of the shell surface
ν	Poisson's ratio
$\boldsymbol{\sigma}$	Column vector of stress components at a point in shell surface

SYMBOLS (Cont'd)

ϕ Angle between meridian and axis (semi-apex angle of cone)

ψ Coordinate transformation matrix (introduced in Equation 11)

INTRODUCTION

A study of the matrix displacement method as applied to the static analysis of shells of revolution is presented. The purpose of the study is to explore in depth the characteristics of the displacement method when applied to the complex shell structure problem, to discuss difficulties, both resolved and unresolved, encountered in the application of the method, and to establish a confidence level in the accuracy of the technique. The latter will be accomplished by a systematic exposition of shell solutions, compared when possible with solutions by other methods. In view of the publication of a number of documents detailing the theoretical background and solution (References 1, 2 and 3) and the associated computer codes (References 4 and 5), only a brief description of the theory and solution method is given for continuity of presentation.

The shell analysis permits arbitrary meridional shapes, axisymmetric and asymmetric distributed and line loading conditions, various boundary conditions, thickness and material property variation in the meridional direction, and stiffening of arbitrary portions of the shell structure, all embodied in the solution of the static response equation:

$$\mathbf{F}^i = \mathbf{K}^i \mathbf{q}^i \tag{1}$$

where $\mathbf{F}^i$ represents the applied generalized forces and reactions, $\mathbf{K}^i$ represents the structural stiffness matrix, and $\mathbf{q}^i$ represents the generalized displacements. In its present form the analysis is limited to homogeneous isotropic single layer (or equivalent multilayer) shells under the assumptions of thin shell theory as formulated by Novozhilov (Reference 6).

A finite element idealization of the structure with completely arbitrary element size is used. The continuous system is represented by a finite number of degrees of freedom in a physically meaningful way with the matrix displacement method used as a simple and straightforward technique for calculating an approximation to the stiffness matrix, $\mathbf{K}^i$, directly.

The application of the displacement method to the analysis of shells of revolution, using conical frusta as the finite elements, was first described by Grafton and Strome (Reference 7), and the idealization has been used by Lu, Penzien, and Popov (Reference 8).

IDEALIZATION OF THE STRUCTURE AND LOADING

The complete shell is idealized into a series of conical frusta joining nodal circles which lie in the shell surface (Figure 1). A right-handed system of cylindrical coordinates is used in the analysis, viz., axial distance z, circumferential angle θ, and radial distance r. The behavior of the shell is characterized by a set of generalized displacements of a nodal circle at station z. These generalized displacements, $\mathbf{q}^i$, are the Fourier coefficients of u, v, w, and β expanded in a Fourier series in θ, where u, v, and w are the axial, circumferential, and radial displacements of a point of the circle, and β is the rotation at the point in a plane containing the axis of the shell and the meridian in the shell surface which passes through the point. The superscript i on $\mathbf{q}^i$ is called the harmonic number.

The corresponding generalized forces may be visualized as representing line loads applied at the nodes and written as

$$\pi r_p T_p(\theta) = \frac{1}{2} Q_p^o + \sum_{i=1}^{m} Q_p^i \cos i\theta + \sum_{i=1}^{m} \bar{Q}_p^i \sin i\theta \qquad (2)$$

where Q_p^i and $\bar{Q}_p^i$ are the generalized forces corresponding to q_p^i and $\bar{q}_p^i$ respectively, r_p is the radius of the p^{th} nodal circle and T_p is an applied load per unit length in a representative direction.

The displacements u, v, and w are positive in the positive directions of z, θ, and r and β is positive if it corresponds to a positive value of $\partial w/\partial z$ along the meridian. The force per unit length, T_p, is positive if it does positive work when displaced through a positive value of q_p.

It may be observed that the generalized forces have been defined so that the total work done by the forces in an incremental displacement (du, dv, dw, $d\beta$) is

$$dW = \sum_j \left\{ Q_j^o \, dq_j^o + \sum_{i=1}^{m} Q_j^i \, dq_j^i + \sum_{i=1}^{m} \bar{Q}_j^i \, d\bar{q}_j^i \right\} , \qquad (3)$$

where the subscript j denotes the generalized coordinate number.

The generalized displacements may be regarded as the independent variables in terms of which the analysis is carried out. If there are n nodes and the highest harmonic number used is m, the system may be said to have 4n(2m + 1) degrees of freedom.

The elastic behavior of the shell element (i.e., the conical frustum) is sufficiently described if the linear relationship between the generalized forces and the generalized displacements of the two adjacent nodal circles can be written. This relationship defines the element stiffness matrix, **k**, which is an N x N square matrix, where N = 16m + 8 characterizing a 2 node system with m being the highest harmonic. The static shell equations for the conical element uncouple in harmonics (reference 1) so that **k** may be partitioned into (8 x 8) squares representing the various harmonics with all off-diagonal partitions null. Thus, a partitioned set of force-displacement relations for each element may be written as

$$\mathbf{Q}^i = \mathbf{k}^i \mathbf{q}^i ; \quad i = 0, \cdots, m \qquad (4)$$

where $\mathbf{k}^i$ is the element stiffness matrix for the i^{th} harmonic. It is to be noted that the relationships between $\bar{Q}^i$ and $\bar{q}^i$ have been left out to simplify the writing. The matrix Q^i is of order (8 x 1), k^i is of order (8 x 8) and q^i is of order (8 x 1).

Assuming the element stiffness matrix is known, a structural stiffness matrix, **K** may be obtained by superposing the element stiffnesses **k**. This is done according to the equilibrium equation in each direction at each node, which equates the applied force to the sum of the forces acting on the elements bounded by the node. It follows, since the respective displacements at a given node are the same for adjacent elements, that each coefficient in **K** is the sum of the corresponding element stiffnesses (Reference 1, Section 3.3). Furthermore, since **k** uncouples in harmonics so does **K** and Equation 1 follows immediately. The $\mathbf{K}^i$ matrices are (4n x 4n) symmetric matrices; the zeroth and first harmonic stiffness matrices are singular due to the rigid-body degrees of freedom of the structure (References 4 and 5).

THE ELEMENT STIFFNESS MATRIX

Once $\mathbf{K}^i$ is available, a solution of Equation 1 follows by solving for the unknown displacements after inverting a nonsingular version of $\mathbf{K}^i$ obtained by eliminating rows and columns corresponding to a given set of displacement boundary conditions (Reference 1, Section 3.3, Reference 4, Section 2.2). As the reactions at the restrained nodes and the stresses at all the nodes are easily calculated once the displacement matrix $\mathbf{q}^i$ is known, it is obvious that the key step in the analysis is the determination of the element stiffness matrix, $\mathbf{k}^i$.

An approximation to the stiffness matrix is calculated by first assuming the following displacement field for the element for harmonic number i:

$$\begin{aligned} \tilde{u}^i &= (\alpha_5^i + \alpha_6^i s) \cos i\theta \\ \tilde{v}^i &= (\alpha_7^i + \alpha_8^i s) \sin i\theta \\ \tilde{w}^i &= (\alpha_1^i + \alpha_2^i s + \alpha_3^i s^2 + \alpha_4^i s^3) \cos i\theta \end{aligned} \tag{5}$$

The displacement components $\tilde{u}^i$, $\tilde{v}^i$, and $\tilde{w}^i$ correspond to shell coordinates and are measured in the plane of the shell surface and normal to it as seen in Figure 1.

If these values for the displacements are substituted in the strain-displacement relations for a conical shell, the following matrix equation relating the strains in the shell and the coefficients $\{\boldsymbol{\alpha}^i\}$ is obtained:

$$\boldsymbol{\epsilon}^i = \mathbf{W}^i \boldsymbol{\alpha}^i \tag{6}$$

where the coefficients $\mathbf{W}^i$ are functions of s and θ.

The stress-strain relations[†] can be written as

$$\boldsymbol{\sigma}^i = \mathbf{E}\, \boldsymbol{\epsilon}^i \tag{7}$$

and it follows that the total strain energy for an element deformed in the assumed manner is[†]

$$U^i = \frac{1}{2} \int_A (\boldsymbol{\alpha}^i)^T (\mathbf{W}^i)^T \mathbf{E}^* \mathbf{W}^i \boldsymbol{\alpha}^i \, dA \tag{8}$$

Defining

$$\mathbf{L}^i = \int_A (\mathbf{W}^i)^T \mathbf{E}^* \mathbf{W}^i \, dA \tag{9}$$

and since the coefficients $\boldsymbol{\alpha}^i$ do not vary over the element,

$$U^i = \frac{1}{2} (\boldsymbol{\alpha}^i)^T \mathbf{L}^i \boldsymbol{\alpha}^i \tag{10}$$

is obtained.

[†]Refer to the Appendix for matrices $\mathbf{E}$ and $\mathbf{E}^*$

The generalized displacements $\mathbf{q}^i$ are the amplitudes of u^i, v^i, w^i, and β^i at the two ends of an element. They can be expressed, in turn, in terms of the amplitudes of $\tilde{u}^i$, $\tilde{v}^i$, $\tilde{w}^i$, and β^i by a simple coordinate transformation matrix $\boldsymbol{\psi}$, i.e.,

$$\mathbf{q}^i = \boldsymbol{\psi}\, \tilde{\mathbf{q}}^i \tag{11}$$

Since

$$\tilde{\mathbf{q}}^i = \mathbf{B}\, \boldsymbol{\alpha}^i \tag{12}$$

where $\mathbf{B}$ is evaluated by substituting the nodal values of s in Equation 5, $\boldsymbol{\alpha}^i$ may be solved for in terms of $\mathbf{q}^i$ using Equations 11 and 12. Substituting for $\boldsymbol{\alpha}^i$ in Equation 10 and comparing the result with the general matrix equation for the strain energy of a linear elastic element, that is,

$$U^i = \frac{1}{2} (\mathbf{q}^i)^T \mathbf{k}^i \mathbf{q}^i \tag{13}$$

it is seen that

$$\mathbf{k}^i = \boldsymbol{\psi} (\mathbf{B}^{-1})^T \mathbf{L}^i \mathbf{B}^{-1} (\boldsymbol{\psi})^T \tag{14}$$

it should be pointed out that the product $(\mathbf{B}^{-1})^T \mathbf{L}^i \mathbf{B}^{-1}$ is the stiffness matrix $\tilde{\mathbf{k}}^i$ referred to shell coordinates $\tilde{\mathbf{q}}^i$.

The $\mathbf{W}^i$, $\mathbf{E}$, $\boldsymbol{\psi}$, and $\mathbf{B}$ matrices are given in the Appendix.

STATIC ANALYSIS PROGRAMS

The construction and solution of Equation 1 for complex shell systems was originally coded in FORTRAN II for an IBM 7094 at the MIT Aeroelastic and Structures Research Laboratory (Reference 5). The computer program, called SABOR III, accepts a description of the structure in terms of the coordinates of the nodal circles and the properties (thickness, Young's modulus, and Poisson's ratio) of the conical elements joining them. For each harmonic in turn, it calculates the unknown displacements $\mathbf{q}^i$ for a given set of external generalized forces applied at the nodal circles and a given set of displacement boundary conditions. Although the method permits an arbitrary boundary displacement, the program is limited to the complete restraint of a node in a particular direction. The program is fully described in a report (Reference 5) and was developed from an earlier program, SABOR I, which handles only axisymmetric deformations (Reference 4). Although an axisymmetric problem corresponds to the zeroth circumferential harmonic which can also be solved by the SABOR III program, it is easier to work with SABOR I when modifying the program and preparing input for axisymmetric cases.

After computing the displacements of the structure, the program calculates the reactions at the restrained nodes by premultiplying the displacements by the appropriate portion of the structural stiffness matrix. It then estimates the shell stress resultants and stress couples at the nodes. Some of these stresses are obtained by direct application of the stress-displacement relations of the conical shell element while some are obtained using the equilibrium equations. The matrix equations and the exact formulas for the stress calculations have been published (see Reference 3, Appendix B).

DEVELOPMENT OF THE SOLUTION

As outlined above, the solution is seen as a straightforward application of the matrix displacement method. It becomes of interest to discuss in detail the unique portions of the

development concerned with the shell of revolution. Problems which have been resolved will be dealt with here, while unresolved problems will be discussed in a subsequent section.

Basic to the matrix displacement method and its application to the conical element is that displacement compatibility at the nodal circles is satisfied exactly, equilibrium at the nodes is satisfied in obtaining $\mathbf{K}^i$, and strain compatibility is satisfied in the interior of the element by using the strain-displacement relations of the conical shell. As the shell stress-strain relations are used in the derivation (Equation 7), all that remains towards satisfaction of all the equations of a conical shell and thus an exact solution for the element stiffness matrix, $\mathbf{k}^i$, is the satisfaction of the shell equilibrium equations in the interior of the element. The degree of approximation to the strain energy, U^i, of the conical element, using the assumed displacement field in Equation 5, determines how well equilibrium is satisfied.

Thus, by improving the original displacement function, such as by including more terms in the polynomial assumption, $\mathbf{k}^i$ can be improved. It has been shown (Reference 9) that if more terms are included, the principle of minimum potential energy may be used to optimize their values, resulting in a better approximation to the stiffness matrix than that obtained using the basic eight-term displacement assumption. Numerical results have been given for conical and cylindrical element stiffness matrices obtained via displacement functions of increasing complexity (Reference 3). In addition, for the case of torsion-free axisymmetric loading, a pertinent although limited study pertaining to number of elements required versus displacement field complexity has shown it is more advantageous to use a larger number of elements with a basic six-term displacement function. This study helped answer the question of how much sophistication should be required in the derivation of $\mathbf{k}^i$ for accurate structural analysis.

In attempting to satisfy the equations of a thin conical shell, the problem as to which shell theory to use becomes important. The differences in various theories are reflected by differences in the strain-displacement relations. In the Appendix, a set of strain-displacement relations derivable from the text of Novozhilov (Reference 6) and a set utilizing Sanders' theory (Reference 10) are presented. These strain-displacement relations differ in a term of the order of the midplane strain to the radius-of-curvature ratio (ϵ/R). The fact that a difference of this nature is not distinguishable in many practical shell problems has been illustrated by a comparison of solutions of cylindrical shells under edge loadings (Reference 3, Appendix C).

The elements of the $\mathbf{L}^i$ matrix (Equation 9) contain integrals of the form

$$A_{\alpha,\beta} = \int_0^{\ell} r^{\alpha} s^{\beta} \, ds \tag{15}$$

For the case of a cylindrical element where r is a constant, the integrals can be expressed in simple formulas. However, the resulting formulas for conical elements with negative powers of r turn out to be ill-conditioned for machine computation when the semi-apex angle, ϕ, of the cone is small (for more details see Reference 1, p. 65). Therefore, in the SABOR programs, these integrals are evaluated by Weddle's seven-point integration formula (Reference 11). The $\mathbf{L}^i$ matrix and the formulas for $A_{\alpha,\beta}$ have been fully tabulated (Reference 3, Appendix A).

It is possible to write Equation 14 in explicit form with the coefficients of $\mathbf{k}^i$ expressed as functions of the geometry of the element and its elastic properties. Grafton and Strome (Reference 7) achieved this at the expense of a consistent development by introducing a further approximation; namely, that all the integrals could be approximated by the "trapezoidal rule," that is,

$$\int_{s_1}^{s_2} f(s)\,ds = \frac{s_2 - s_1}{2}\left(f(s_2) + f(s_1)\right) \qquad (16)$$

Although this leads to an acceptable approximation to $\mathbf{k}^o$ for many purposes as shown in examples presented by Grafton and Strome, a consistently integrated formulation allows the same accuracy of solution to be achieved with fewer structural elements (Reference 1, p. 73, Figure 13).

In this particular application of the finite element approach, two further problems present themselves: the effect of approximating shell meridional curves by conical frusta, i.e., linear meridional segments, and the effect of approximating distributed surface loads by circumferential line loads applied at the nodal circles.

As a beginning to this discussion, a 35-element solution for the meridional moment (note the sign convention for shell stress resultants given in Figure 2) in a cylindrical shell under edge loads (Figure 3) is presented. This solution contains neither of these approximations and gives four decimal place agreement with a solution by Lu, Penzien and Popov (Reference 8). A convergence study using 15 and 20 elements gives almost identical results and although there exists no general convergence proof for the finite element approach, for this and many other examples attempted (Reference 3) using the conical element, all results converge to solutions obtained by other methods when the number of elements is increased. In this study, such converging results will be assumed accurate.

Considering a circular plate under axisymmetric pressure loading (Figure 4), the structure is modeled exactly by the conical elements as in the previous example, but the loading is approximated by lumping at each node half the total force on each element adjacent to it. The convergence study presented for 5, 10, 20, and 40 elements indicates that the latter three idealizations converge for displacements and stresses and even the crude five element breakdown gives reasonable results. Although the matrix displacement method usually gives better values for displacements than for stresses, the excellent results for stresses are a consequence of the constant geometry and properties, the lack of large displacement gradients between successive nodes, and the exact modeling of the plate (no discontinuity in slope of of the shell's meridian).

Interpreting these results requires noting that there are two values of stress for the two elements meeting at a node and the lack of noticeable difference on the scale used indicates the accuracy in which force equilibrium is satisfied at each node. The discontinuous meridional shear curve for the 40-element case points this out clearly as the two values at each node add up to the applied external force at the node when the sign convention is taken into account. The 5, 10, and 20-element cases for the meridional shear (not shown) give a larger discontinuity at each node as the applied forces are larger. In all cases, the average nodal value approximates the correct result in the real structure which has a continuous distribution of load and thus no discontinuity in stress.

In an attempt to illustrate both approximations under discussion, solutions of spherical and parabolic caps under axisymmetric pressure loading are presented (Figure 5). These shells have the exact same thickness, material properties and pressure loading as the above plate example, and have fixed ends at the same radial distance. The convergence of stresses and displacements is very similar to the convergence noted in the plate results, although the meridional moment shows an unrealistic trend near the center of the cap for the 14-element case. A singularity in stress occurs when the radius approaches zero and the convergence study shows this effect can be made negligible by using more elements. If more elements

are not available, another solution is the use of a 3 x 3 stiffness matrix for a circular plate in a small region at the shell's apex (Reference 3). In general this stress singularity damps out within a few elements from the apex.

The spherical cap solution compares reasonably well with a finite difference solution for the meridional moment (Figure 5) used in a report by Koval and Bhuta (Reference 12) for comparison with a dynamic solution (not shown here), the latter including damping to decay the response to the static condition. The dynamic solution compares almost exactly with the finite element convergence study. It is interesting that although a plot of the finite element model of the sphere and parabola for all idealizations presented shows no significant differences between the curves, the finite element solution gives different displacement and stress curves for the two shells, graphically demonstrating the accuracy of the calculations.

Although it has been shown that excellent results may be obtained within the framework of load and shell shape approximations, these results have been for plates and shallow shells. For shells with greater curvature, the problem of residual meridional bending moments, as first mentioned by Lu, Penzien, and Popov (Reference 8), becomes important. In their report, the finite element approach for shells of revolution under axisymmetric loads is used with an element stiffness matrix derived from an exact solution of a conical frustum under edge loads.

RESIDUAL MOMENTS

A convergence study for a 75-degree spherical cap under axisymmetric pressure loading (Figure 6) agrees with a similar solution given by Lu, Penzien, and Popov (Reference 8), although both exhibit a residual moment in the membrane region. Comparison with Hetenyi's solution (Reference 13) indicates these results are in error. It is clear that these residual moments become less pronounced when the elements are reduced in size. In a similar shell solution where a 35-degree nonshallow spherical cap under pressure (Reference 3, Figure 5) was idealized as 35 one-degree elements, this smaller element size resulted in excellent agreement with the hypergeometric series solution and negligible residual moments.

Since the use of a large number of elements is not the best solution to this problem because of the possible necessity of allocating many elements to regions where discontinuities in geometry and large gradients in loading occur, another solution is sought. Consider a toroidal shell (Figure 7) analyzed for 20, 28, and 42 elements and compared with a solution given by Popov and Lu (Reference 14). The shell is fixed at one end and solutions are given for an axial compressive load at the free edge and for gravity loading. Good correlation is obtained with the 84-element solutions given by Popov and Lu, with their slightly better results due to their use of twice the number of elements. In the 42-element axially-loaded shell in which no loading approximation is made, a small residual moment shows that this difficulty is due at least in part to the shell shape approximation. In the gravity loaded shell, there is a slightly larger residual moment but not nearly as pronounced as in the pressure loaded spherical shell indicating that the loading approximation has some effect which becomes worse for loadings normal to the shell than for those oriented in a direction closer to a tangent to the shell's meridian.

The fact that a residual moment, although small, is seen in a 42-element toroidal shell without a load approximation, while this effect is not noticeable in a 10-element plate and a 27-element shallow sphere, which have a pressure load approximation, is strong evidence that the meridional approximation is a major reason for the residual moment. An element stiffness matrix for a curved finite element in the meridional direction has been derived (Reference 1), and a method is also available for consistently estimating distributed loads on finite elements utilizing the same displacement field as in Equation 5 (Reference 15).

At present there are no numerical results available in either of these areas, and although work is in progress, it should be emphasized that the residual moment effect is a minor problem and one correctable by increasing the number of elements.

In this discussion of residual moments, the question as to how well a structural analysis using an approximate stiffness matrix derived from assumed displacements compares with an exact solution for this stiffness matrix has been indirectly answered. The above examples compared with solutions by Lu, Penzien, and Popov are another indication that the basic eight-term displacement function was sufficient for the derivation of k^i.

NUMBER OF FINITE ELEMENTS

The number of finite elements available is important not only for eliminating residual moments but for analyzing certain complex structures with rapidly varying surface loads. At present the SABOR programs are limited to 50 elements for the axisymmetric problem and 40 elements for the asymmetric problem. The solution of Equation 1 is accomplished by direct inversion of the stiffness matrix K^i, which takes up most of the core storage of the IBM 7094 and which preserves an approximate 10 to 1 ratio of zero to nonzero terms.

For a system of simultaneous equations represented in Equation 1 in which the K^i matrix is symmetric and positive definite, it is possible to solve a system of 800 equations representing 200 finite elements for the asymmetric problem. This figure is approximate and may be increased or decreased depending on many factors such as whether the IBM 7094 computations are done in double or single precision, the position of off-diagonal terms, etc. The solution method entails factoring the K^i matrix into upper and lower triangular forms which are the transpose of each other and which preserve all the zeros in the original matrix (only the nonzero elements of one factor are stored). The factors are then used successively in two simplified solutions of the simultaneous equations which require only algebraic manipulation. This procedure is similar to Cholesky's method (Reference 11) and is extremely fast and efficient.

DISCUSSION AND CONCLUSIONS

This study has been simplified by certain modifications and extensions of the SABOR codes*. The input is concise and relatively straightforward. The output lists the geometry, material properties, and reactions of the structure. Stresses, strains, and displacements are calculated for each harmonic, superimposed at any value of circumferential angle, printed, and automatically plotted in terms of axial, radial, or meridional distance at option. The curves presented in this study have been taken from such machine plots.

The SABOR codes have been used for complex shell structures with the same facility as for the relatively simple shells previously discussed. In an axisymmetric deformation problem (Figure 8), the axial displacement converges very well for various finite element models. SABOR permits an arbitrary axisymmetric stiffness at any node in any direction, which is very well illustrated by the radial displacement curve. Increasing the radial stiffness at node 31 (z = 34.15 in., r = 9.96 in.) decreases the radial displacement in successive steps to the limiting case of zero radial displacement. In an asymmetric response problem (Figure 9), 31 Fourier harmonics are used to approximate the load function. The displacement curves

*The author wishes to express his thanks to Mr. G. Urmston of the Computation and Mathematics Center, Aerospace Corporation, San Bernardino Operations, California, for his continuing efforts in modifying and improving the SABOR codes.

are found by superimposing the Fourier coefficients of displacements at the desired values of circumferential angle. In both complex shells, values of thickness and Young's Modulus vary from element to element and as a result the stress resultants (not shown) are not expected to be as accurate nor do they converge as well as in previous examples.

Considering the complexities of the shell problems under discussion, it is of interest to mention the machine computation time required by the SABOR programs. Except possibly for the time to prepare input, the more complex structures require no more machine time than the simple shells for an equivalent number of degrees of freedom. An empirical curve (Figure 10) constructed from a large number of computer runs indicates that 0.2 to 1.7 minutes are required per individual harmonic. The maximum time is used for the 164-degree of freedom upper limit in the present version of SABOR III. It should be noted that the original FORTRAN II SABOR code has been rewritten in FORTRAN IV and this has reduced the running time considerably. Although the time required for an axisymmetric (zeroth harmonic) solution or any individual harmonic solution is small, a problem requiring many harmonics for a slowly converging Fourier representation of the load may necessitate a large amount of machine time. For example, the 36-element - 148-degree of freedom complex structure (Figure 9) required 51 minutes on the IBM 7094 for the 31 harmonic solution. This time will be greatly reduced by the same method contemplated for increasing the number of finite elements allowed.

In conclusion, it must be emphasized that this paper was intended to give an in-depth presentation of the particular application of the matrix displacement finite element approach to the analysis of shells of revolution. Details of problem areas encountered in the development of the method, solutions of complex structures, studies of the convergence of various shell solutions, improvements in the codes already made and those contemplated, machine time required, etc., are all designed to enable the researcher to get a feel for the background efforts in this work. This is especially important as work is continuing in other areas of structural analysis using the linear elastic analysis in SABOR as a basis. Successful efforts are being made in dynamic analysis, free and forced vibration solutions, buckling analysis, and plastic analysis in addition to increasing the scope of the present solution to handle anisotropic-orthotropic and double layer-multilayer shells of revolution.

REFERENCES

1. Klein, S., Matrix Analysis of Shell Structures, S. M. Thesis, Report No. ASRL-TR-121-12, Department of Aeronautics and Astronautics, MIT, Cambridge, Mass., June 1964.

2. Percy, J. H., Pian, T. H. H., Klein, S., and Navaratna, D. R., Application of Matrix Displacement Method to Linear Elastic Analysis of Shells of Revolution, AIAA Paper No. 65-142. Presented at the AIAA Second Aerospace Sciences Meeting, New York, N. Y., 25-27 January 1965.

3. Percy, J. H., Pian, T. H. H., Navaratna, D. R., and Klein, S., Application of the Matrix Displacement Method to the Linear Elastic Analysis of Shells of Revolution, ASRL-TR-121-7, Aeroelastic and Structures Research Laboratory, MIT, Cambridge, Mass., January 1965.

4. Percy, J. H., Navaratna, D. R., and Klein, S., SABOR I: A FORTRAN Program for the Linear Elastic Analysis of Thin Shells of Revolution under Axisymmetric Loading by Using the Matrix Displacement Method, TR-121-5, Aeroelastic and Structures Research Laboratory, MIT, Cambridge, Mass., April 1965.

5. Percy, J. H., Navaratna, D. R., and Klein, S., SABOR III: A FORTRAN Program for the Linear Elastic Analysis of Thin Shells of Revolution under Asymmetric or Axisymmetric Loading by Using the Matrix Displacement Method, TR-121-6, Aeroelastic and Structures Research Laboratory, MIT, Cambridge, Mass., May 1965.

6. Novozhilov, V. V., Theory of Thin Shells (Translation, P. Noordhoff, p. 24, 1959).

7. Grafton, P. E., and Strome, D. R., "Analysis of Axisymmetric Shells by the Direct Stiffness Method," AIAA Journal, Vol. 1, pp. 2342-2347, 1963.

8. Lu, Z. A., Penzien, J., and Popov, E. P., Finite Element Solution for Thin Shells of Revolution, NASA CR-37, July 1964.

9. Pian, T. H. H., "Derivation of Element Stiffness Matrices," AIAA Journal, Vol. 2, pp. 576-577, 1964.

10. Sanders, J. L., Jr., An Improved First-Approximation Theory for Thin Shells, NASA TR R-24, 1959.

11. Salvadori, M. G., Baron, M. L., Numerical Methods in Engineering, Prentice-Hall, Inc., New Jersey, 1961.

12. Koval, L. R., and Bhuta, P. G., Dynamic Response of Shallow Spherical Shells, EM 13-21, TRW Space Technology Laboratories, October 1963.

13. Hetenyi, M. I., Beams on Elastic Foundations, University of Michigan Press, Ann Arbor, Mich., 1946.

14. Popov, E.P., and Lu, Z. A., Edge Disturbances in Axisymmetrical Shells of Revolution, I. E. R. Technical Report SESM 64-3, Univ. of California, Berkeley, Calif., September 1964.

15. Archer, J. S., Consistent Matrix Formulations for Structural Analysis Using Influence-Coefficient Techniques, AIAA Preprint No. 64-488. Paper presented at 1st AIAA Annual Meeting, Washington, D. C., 29 June-2 July 1964.

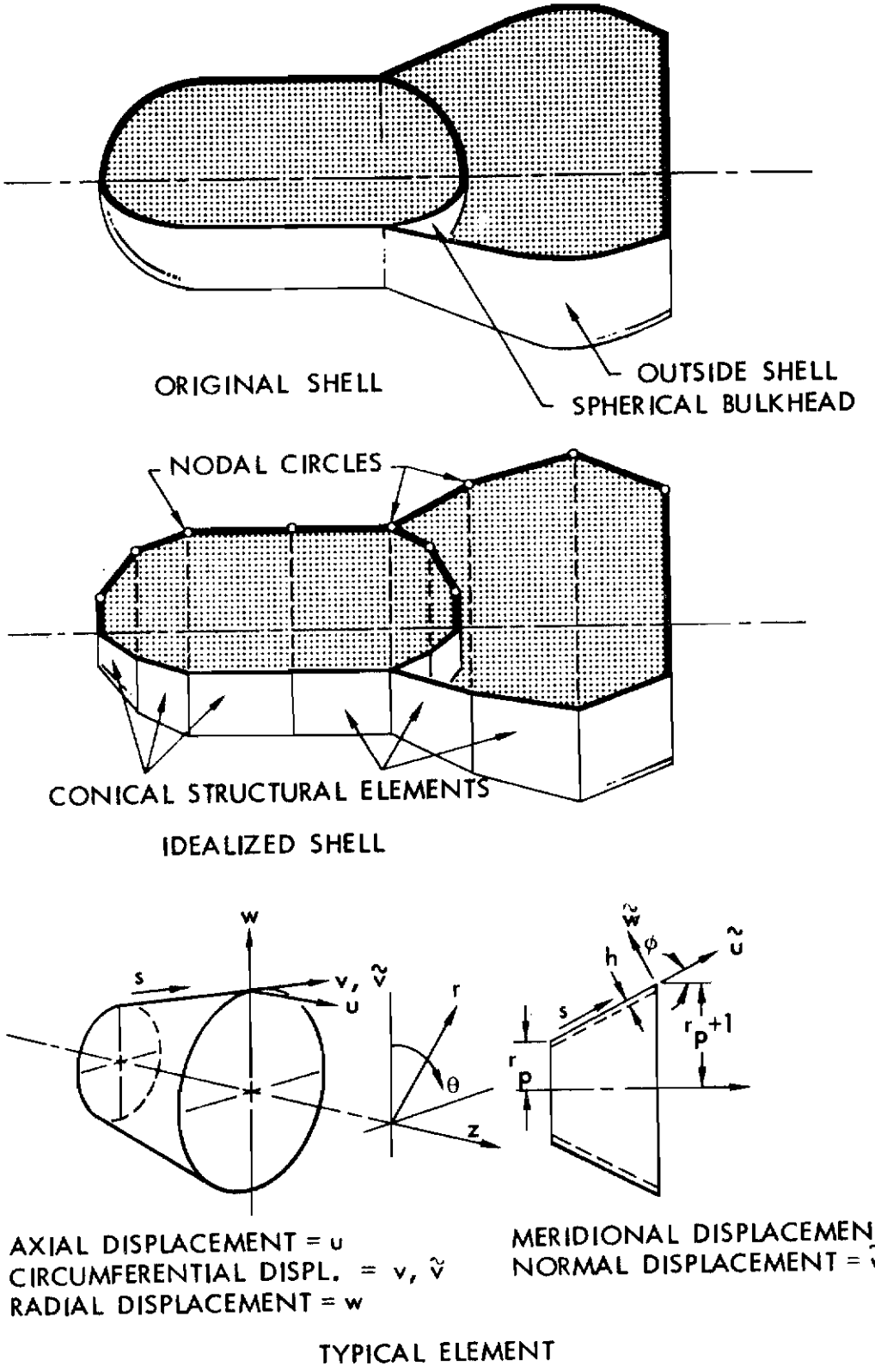

Figure 1. Diagrams to Illustrate the Idealization of a Shell of Revolution for Analysis

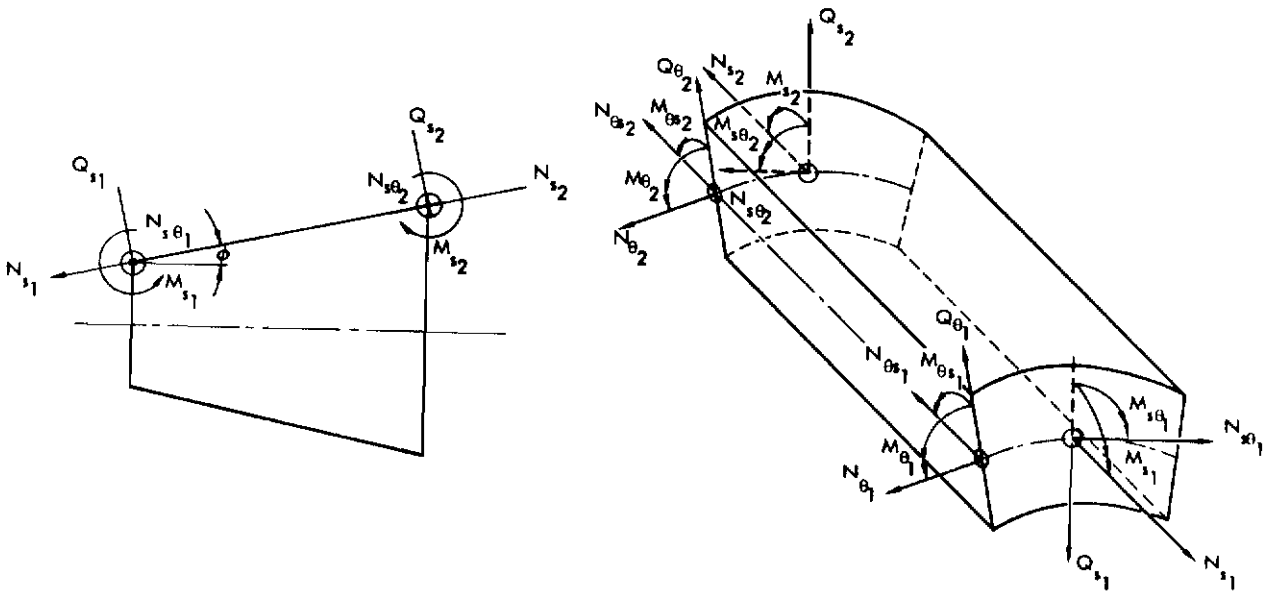

Figure 2. Stress Resultants in Shell Coordinates

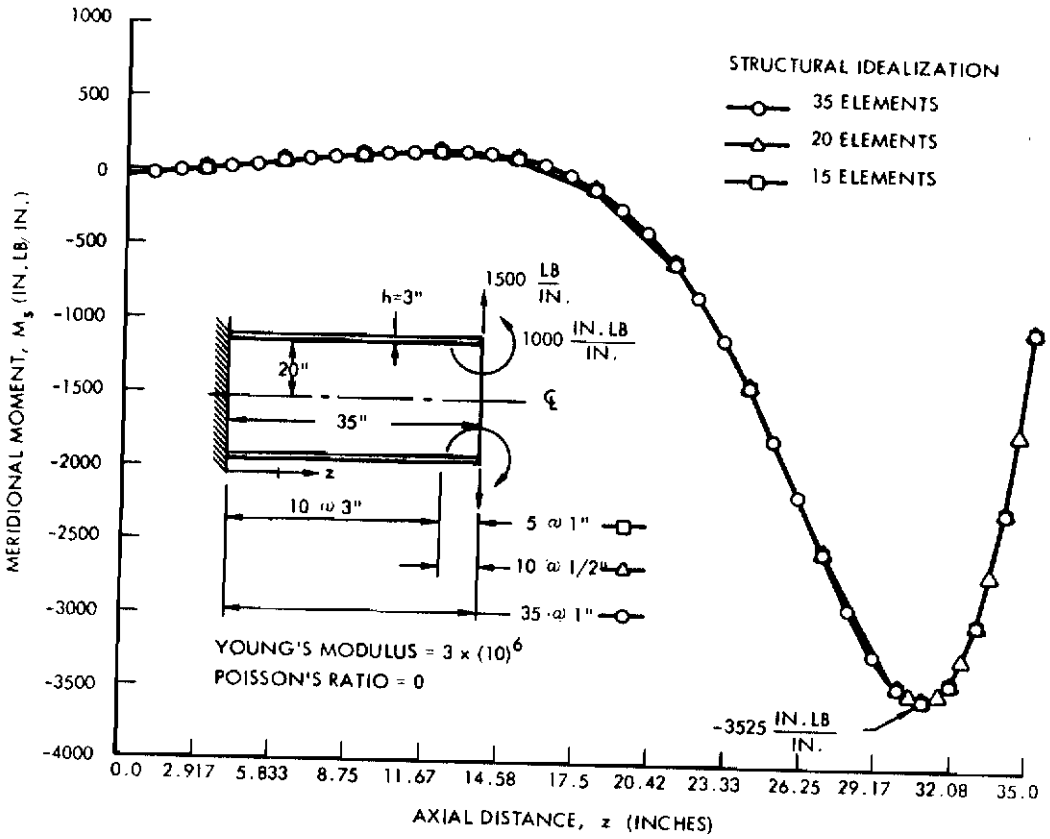

Figure 3. Cylinder Under Edge Loading

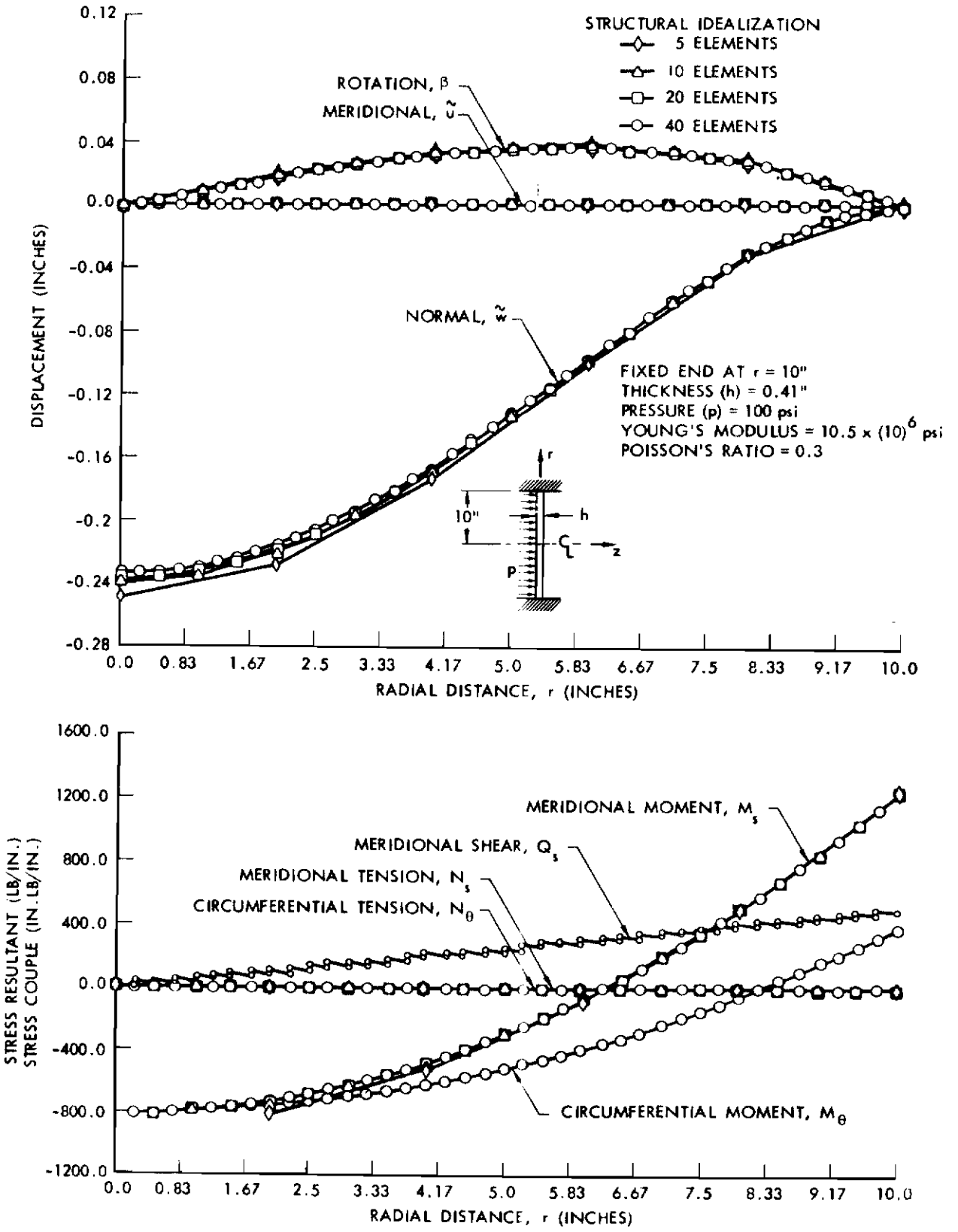

Figure 4. Circular Flat Plate Under Axisymmetric Pressure Loading

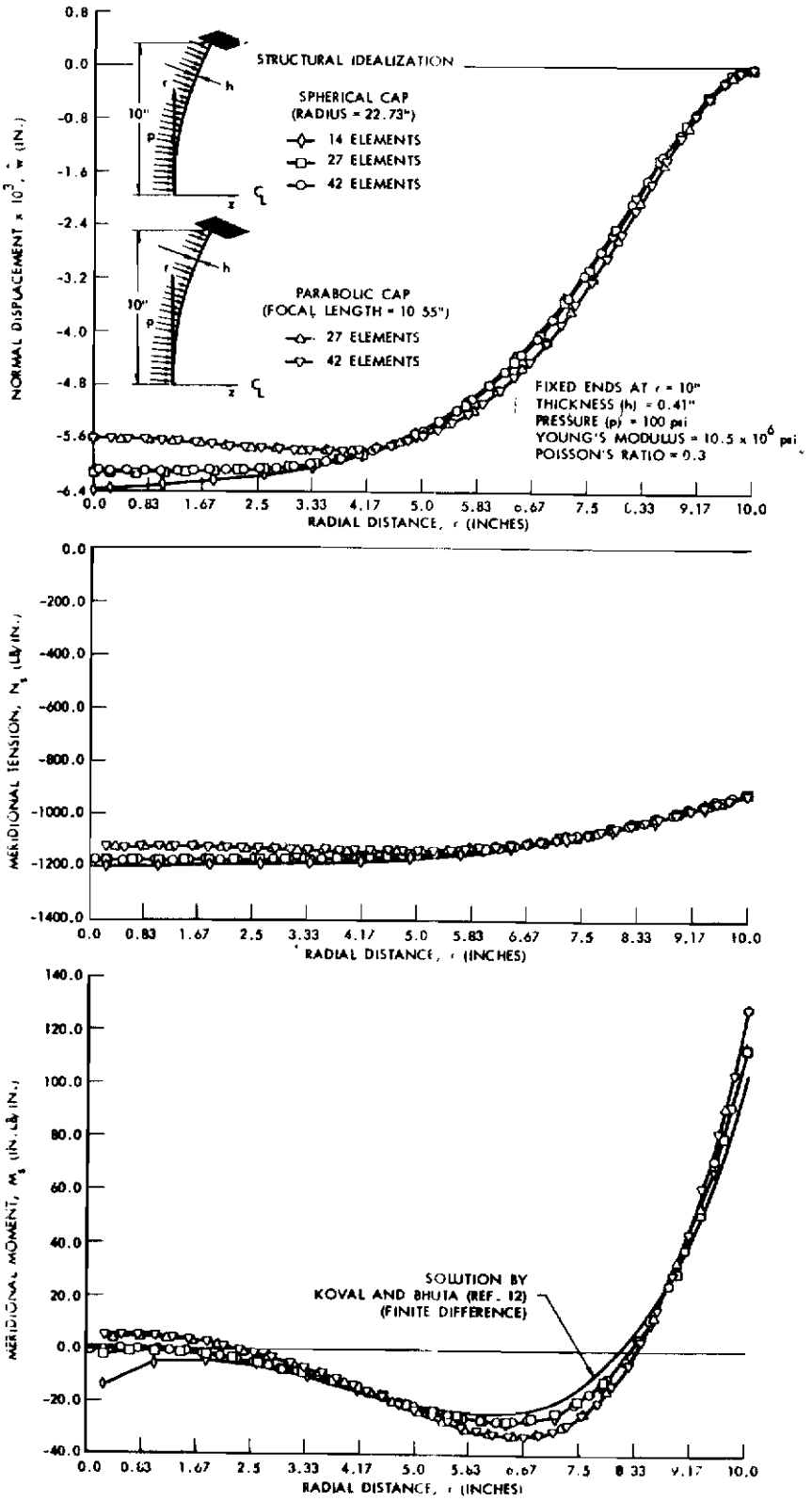

Figure 5. Spherical and Parabolic Shallow Caps Under Axisymmetric Pressure Loading

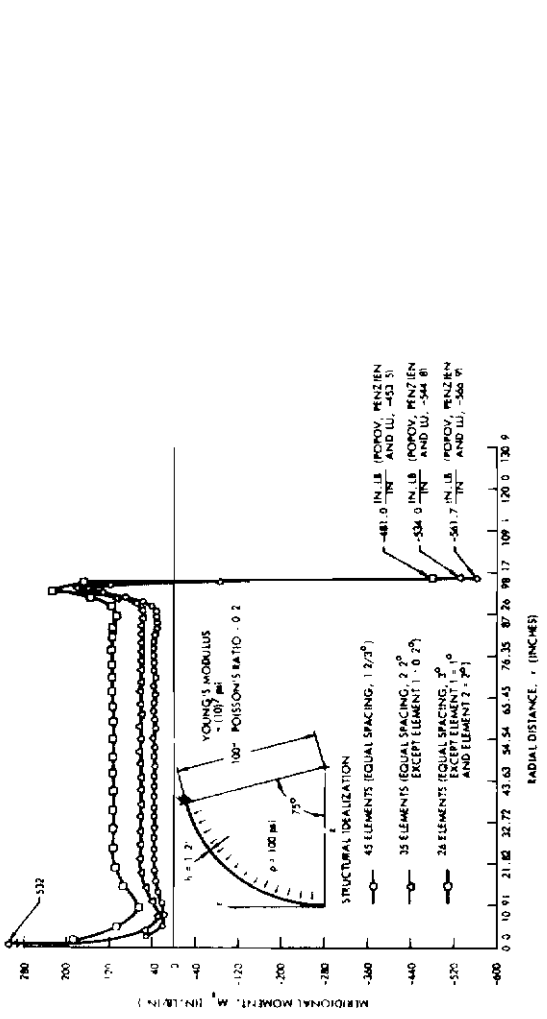

Figure 6. Spherical Cap (75°) Under Axisymmetric Pressure Loading

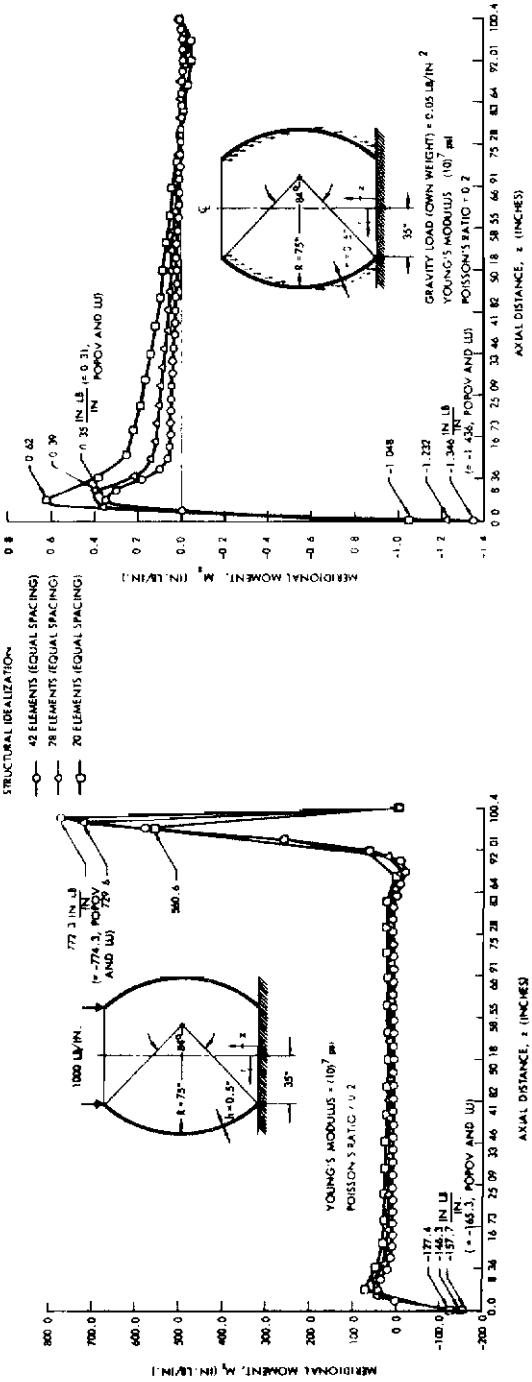

Figure 7. Toroidal Shell Under Gravity Loading and Edge Axial Compressive Load

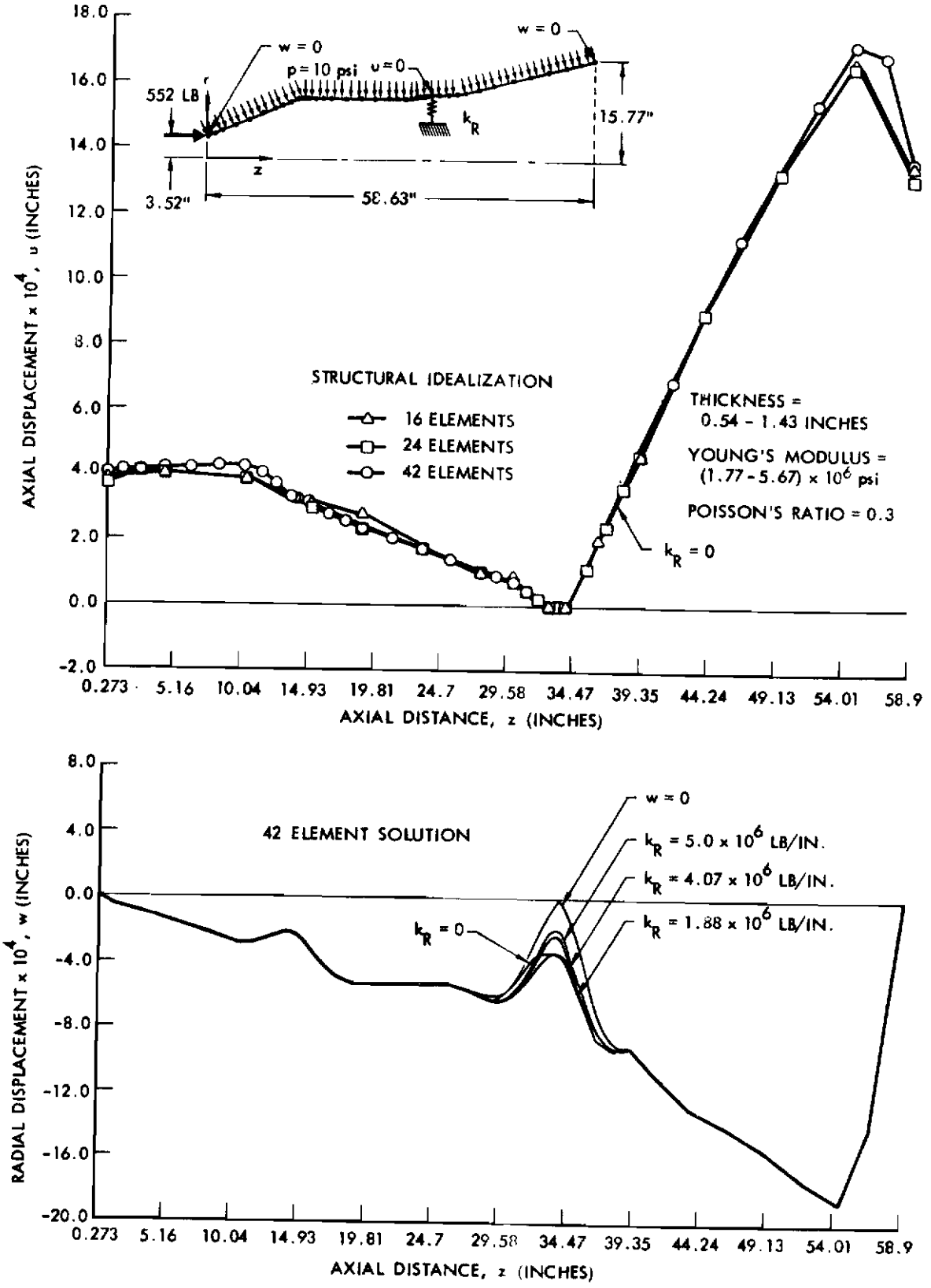

Figure 8. Complex Shell Structure Under Axisymmetric Loading

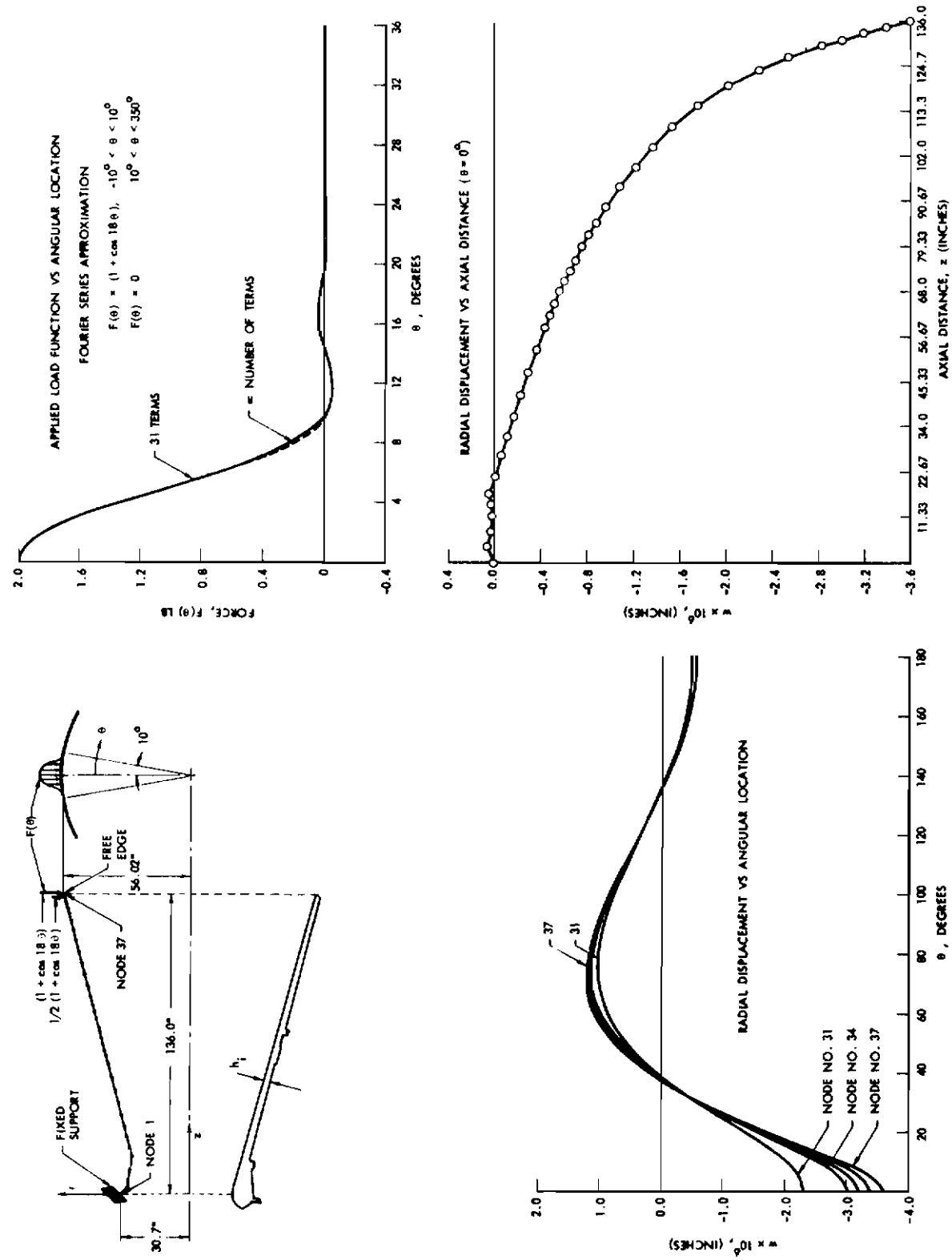

Figure 9. Complex Shell Structure Under Asymmetric Loading

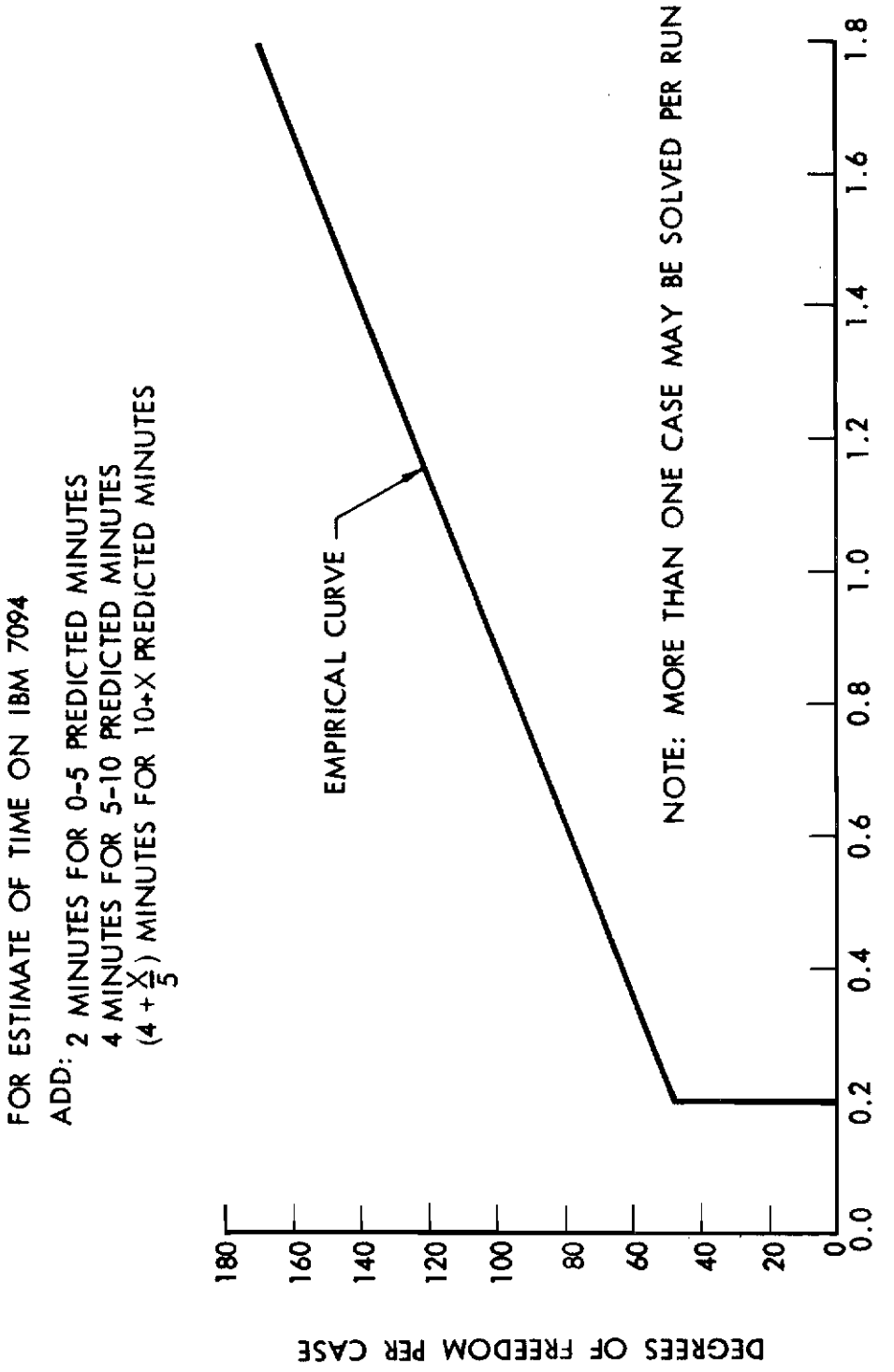

Figure 10. Computation Time for SABOR Runs on IBM 7094

APPENDIX

LIST OF BASIC SHELL EQUATIONS AND VARIOUS MATRICES

In this appendix are listed the basic equations for thin conical shells and the various matrices referred to in the text of the paper.

Strain-Displacement Relations for a Thin Conical Shell (Novozhilov)

$$
\begin{aligned}
\epsilon_s &= \frac{\partial \tilde{u}}{\partial s} \\
\epsilon_\theta &= \frac{1}{r}\frac{\partial \tilde{v}}{\partial \theta} + \frac{\tilde{u}\sin\phi}{r} + \frac{\tilde{w}\cos\phi}{r} \\
\epsilon_{s\theta} &= \frac{1}{2}\left[\frac{1}{r}\frac{\partial \tilde{u}}{\partial \theta} + \frac{\partial \tilde{v}}{\partial s} - \frac{\tilde{v}\sin\phi}{r}\right] \\
\kappa_s &= -\frac{\partial^2 \tilde{w}}{\partial s^2} \\
\kappa_\theta &= -\frac{1}{r^2}\frac{\partial^2 w}{\partial \theta^2} + \frac{\cos\phi}{r^2}\frac{\partial \tilde{v}}{\partial \theta} - \frac{\sin\phi}{r}\frac{\partial \tilde{w}}{\partial s} \\
\kappa_{s\theta} &= -\frac{1}{r}\frac{\partial^2 \tilde{w}}{\partial s\,\partial \theta} + \frac{\sin\phi}{r^2}\frac{\partial \tilde{w}}{\partial \theta} + \frac{\cos\phi}{r}\frac{\partial \tilde{v}}{\partial s} - \frac{\sin\phi\cos\phi}{r^2}\tilde{v}
\end{aligned}
\tag{A.1}
$$

where ϵ_s, ϵ_θ, and $\epsilon_{s\theta}$ are the normal and the shear strains of the middle surface of the shell; κ_s, κ_θ, $\kappa_{s\theta}$ are the curvature changes of the middle surface of the shell, and ϕ is the angle between the meridian and the axis of the shell (semi-angle at vertex of cone). For Sanders' theory (Reference 10) all the strain-displacement relations are the same as above except $\kappa_{s\theta}$ which is given by

$$
\begin{aligned}
\kappa_{s\theta} = &-\frac{1}{r}\frac{\partial^2 \tilde{w}}{\partial s\,\partial \theta} + \frac{\sin\phi}{r^2}\frac{\partial \tilde{w}}{\partial \theta} + \frac{3}{4}\frac{\cos\phi}{r}\frac{\partial \tilde{v}}{\partial s} - \frac{3}{4}\frac{\sin\phi\cos\phi}{r^2}\tilde{v} \\
&- \frac{1}{4}\frac{\cos\phi}{r^2}\frac{\partial \tilde{u}}{\partial \theta}
\end{aligned}
\tag{A.1a}
$$

Stress-Strain Relations for a Thin Conical Shell

$$\left\{N_s \;\; N_\theta N_{s\theta} \; M_s \;\; M_\theta \, M_{s\theta}\right\} = \mathbf{E} \quad \left\{\epsilon_s \, \epsilon_\theta \, \epsilon_{s\theta} \; \kappa_s \, \kappa_\theta \, \kappa_{s\theta}\right\}$$

where

$$\mathbf{E} = \begin{bmatrix} \frac{Eh}{1-\nu^2} & \frac{\nu Eh}{1-\nu^2} & 0 & 0 & 0 & 0 \\ \frac{\nu Eh}{1-\nu^2} & \frac{Eh}{1-\nu^2} & 0 & 0 & 0 & 0 \\ 0 & 0 & \frac{Eh}{1+\nu} & 0 & 0 & 0 \\ 0 & 0 & 0 & \frac{Eh^3}{12(1-\nu^2)} & \frac{\nu Eh^3}{12(1-\nu^2)} & 0 \\ 0 & 0 & 0 & \frac{\nu Eh^3}{12(1-\nu^2)} & \frac{Eh^3}{12(1-\nu^2)} & 0 \\ 0 & 0 & 0 & 0 & 0 & \frac{Eh^3}{12(1+\nu)} \end{bmatrix}$$

and

N_s, N_θ, and $N_{s\theta}$ are stress resultants

M_s, M_θ, and $M_{s\theta}$ are stress couples

E = Young's Modulus

ν = Poisson's Ratio

h = Shell thickness

The matrix $\mathbf{E}^*$ appearing in Equation 8 is formed from the above $\mathbf{E}$ matrix by multiplying the elements $Eh/(1+\nu)$ and $Eh^3/12(1+\nu)$ by a factor of 2; this leads to consistency with the present definitions of $\epsilon_{s\theta}$ and $\kappa_{s\theta}$.

The Matrices ψ and B (Equations 11 and 12)

$$\Psi = \begin{bmatrix} \cos\phi & 0 & -\sin\phi & 0 & 0 & 0 & 0 & 0 \\ 0 & 1 & 0 & 0 & 0 & 0 & 0 & 0 \\ \sin\phi & 0 & \cos\phi & 0 & 0 & 0 & 0 & 0 \\ 0 & 0 & 0 & 1 & 0 & 0 & 0 & 0 \\ 0 & 0 & 0 & 0 & \cos\phi & 0 & -\sin\phi & 0 \\ 0 & 0 & 0 & 0 & 0 & 1 & 0 & 0 \\ 0 & 0 & 0 & 0 & \sin\phi & 0 & \cos\phi & 0 \\ 0 & 0 & 0 & 0 & 0 & 0 & 0 & 1 \end{bmatrix}$$

$$B = \begin{bmatrix} 0 & 0 & 0 & 0 & 1 & 0 & 0 & 0 \\ 0 & 0 & 0 & 0 & 0 & 0 & 1 & 0 \\ 1 & 0 & 0 & 0 & 0 & 0 & 0 & 0 \\ 0 & 1 & 0 & 0 & 0 & 0 & 0 & 0 \\ 0 & 0 & 0 & 0 & 1 & \ell & 0 & 0 \\ 0 & 0 & 0 & 0 & 0 & 0 & 1 & \ell \\ 1 & \ell & \ell^2 & \ell^3 & 0 & 0 & 0 & 0 \\ 0 & 1 & 2\ell & 3\ell^2 & 0 & 0 & 0 & 0 \end{bmatrix}$$

W^1 Matrix (Equation 6)

where $[W^i]$ can be expressed as

$$W^i = \begin{bmatrix} \cos i\theta & 0 & 0 & 0 & 0 & 0 \\ 0 & \cos i\theta & 0 & 0 & 0 & 0 \\ 0 & 0 & \sin i\theta & 0 & 0 & 0 \\ 0 & 0 & 0 & \cos i\theta & 0 & 0 \\ 0 & 0 & 0 & 0 & \cos i\theta & 0 \\ 0 & 0 & 0 & 0 & 0 & \sin i\theta \end{bmatrix} \begin{bmatrix} 0 & 0 & 0 & 0 & 0 & 0 \\ \frac{\cos\phi}{r} & \frac{s\cos\phi}{r} & \frac{s^2\cos\phi}{r} & \frac{s^3\cos\phi}{r} & \frac{\sin\phi}{r} & \frac{si}{r} \\ 0 & 0 & 0 & 0 & \frac{-i}{2r} & \frac{-si}{2r} & \frac{-\sin\phi}{2r} & \left(\frac{1}{2}-\frac{s\sin\phi}{2r}\right) \\ 0 & 0 & -2 & -6s & 0 & 0 & 0 & 0 \\ \frac{i^2}{r^2} & \left(\frac{si^2}{r^2}-\frac{\sin\phi}{r}\right) & \left(\frac{s^2i^2}{r^2}-\frac{2s\sin\phi}{r}\right) & \left(\frac{s^3i^2}{r^2}-\frac{3s^2\sin\phi}{r}\right) & 0 & 0 & \frac{i\cos\phi}{r^2} & \frac{si\cos\phi}{r^2} \\ \frac{-i\sin\phi}{r^2} & \left(\frac{i}{r}-\frac{is\sin\phi}{r^2}\right) & \left(\frac{2si}{r}-\frac{s^2i\sin\phi}{r^2}\right) & \left(\frac{3s^2i}{r}-\frac{s^3i\sin\phi}{r^2}\right) & 0 & 0 & \frac{-\sin\phi\cos\phi}{r^2} & \left(\frac{1}{r}-\frac{s\sin\phi}{r^2}\right)\cos\phi \end{bmatrix}$$

and $[W^i]$ may be formed from $[W^i]$ by writing -i for i.